



**HAL**  
open science

# An aqueous zinc-ion battery working at $-50^{\circ}\text{C}$ enabled by low-concentration perchlorate-based chaotropic salt electrolyte

Guoshen Yang, Jialei Huang, Xuhao Wan, Binbin Liu, Yachao Zhu, Jiawei Wang, Olivier Fontaine, Shiqiang Luo, Pritesh Hiralal, Yuzheng Guo, et al.

► **To cite this version:**

Guoshen Yang, Jialei Huang, Xuhao Wan, Binbin Liu, Yachao Zhu, et al.. An aqueous zinc-ion battery working at  $-50^{\circ}\text{C}$  enabled by low-concentration perchlorate-based chaotropic salt electrolyte. *EcoMat*, 2022, e12165, 10.1002/eom2.12165 . hal-03538020

**HAL Id: hal-03538020**

**<https://hal.umontpellier.fr/hal-03538020>**

Submitted on 2 Mar 2022

**HAL** is a multi-disciplinary open access archive for the deposit and dissemination of scientific research documents, whether they are published or not. The documents may come from teaching and research institutions in France or abroad, or from public or private research centers.


L'archive ouverte pluridisciplinaire **HAL**, est destinée au dépôt et à la diffusion de documents scientifiques de niveau recherche, publiés ou non, émanant des établissements d'enseignement et de recherche français ou étrangers, des laboratoires publics ou privés.



Distributed under a Creative Commons Attribution 4.0 International License

## RESEARCH ARTICLE

# An aqueous zinc-ion battery working at $-50^{\circ}\text{C}$ enabled by low-concentration perchlorate-based chaotropic salt electrolyte

Guoshen Yang<sup>1</sup> | Jialei Huang<sup>1</sup> | Xuhao Wan<sup>2</sup> | Binbin Liu<sup>1</sup> | Yachao Zhu<sup>3</sup> | Jiawei Wang<sup>1</sup> | Olivier Fontaine<sup>3,4,5</sup> | Shiqiang Luo<sup>6</sup> | Pritesh Hiralal<sup>6</sup> | Yuzheng Guo<sup>2</sup> | Hang Zhou<sup>1</sup> 

<sup>1</sup>School of Electronic and Computer Engineering, Peking University Shenzhen Graduate School, Shenzhen, China

<sup>2</sup>School of Electrical Engineering and Automation, Wuhan University, Wuhan, China

<sup>3</sup>Institute Charles Gerhardt Montpellier, Université Montpellier, Montpellier, France

<sup>4</sup>School of Energy Science and Engineering, Vidyasirimedhi Institute of Science and Technology (VISTEC), Rayong, Thailand

<sup>5</sup>Institut Universitaire de France, Paris, France

<sup>6</sup>Zinergy Shenzhen Ltd., Gangzhilong Science Park, Shenzhen, China

## Correspondence

Yachao Zhu, Institute Charles Gerhardt Montpellier, UMR 5253, Université Montpellier, Montpellier CC 1502, France. Email: yachao.zhu@umontpellier.fr

Yuzheng Guo, School of Electrical Engineering and Automation, Wuhan University, Wuhan, Hubei 430072, China. Email: yguo@whu.edu.cn

Hang Zhou, School of Electronic and Computer Engineering, Peking University Shenzhen Graduate School, Shenzhen 518055, China. Email: zhouh81@pkusz.edu.cn

## Funding information

Guangdong Basic and Applied Basic Research Foundation, Grant/Award Number: 2020A1515010716; Guangdong Introducing Innovative and Entrepreneurial Teams Program, Grant/Award Number: 2019ZT08Z65; Shenzhen Science and Technology Innovation Committee, Grant/Award Numbers: JCYJ20190806145609284, GJHZ201908200912036, JSGG20201102161000002; Shenzhen Science and Technology Program, Grant/Award Number: KQTD20190929172522248

## Abstract

Rechargeable aqueous zinc-ion batteries (ZIBs) have been considered as a promising candidate for the large-scale energy storage device owing to their low cost and high safety. However, the practical application of aqueous ZIBs at low temperature environment is hindered by the freezing aqueous electrolytes, which leads to a sharp drop in ionic conductivity, and thereby a rapid deterioration of battery performance. Herein, a chaotropic salt electrolyte based on low concentration aqueous  $\text{Zn}(\text{ClO}_4)_2$  with superior ionic conductivity under low temperature (4.23 mS/cm at  $-50^{\circ}\text{C}$ ) is reported. The anti-freezing methodology introduced here is completely different from conventional freeze-resistant design of using “water-in-salt” electrolyte, cosolvents, or anti-freezing agent additives strategy. Experimental analysis and molecular dynamics simulations reveal that the as-prepared  $\text{Zn}(\text{ClO}_4)_2$  electrolyte possesses faster ionic migration compared with other commonly used Zn-based salts (i.e.,  $\text{Zn}(\text{CF}_3\text{SO}_3)_2$  and  $\text{ZnSO}_4$ ) electrolyte. It is found that  $\text{Zn}(\text{ClO}_4)_2$  electrolyte can suppress the ice crystal construction by forming more hydrogen bonds between solute  $\text{ClO}_4^-$  and solvent  $\text{H}_2\text{O}$  molecules, thus leading to a superior anti-freezing property. The fabricated ZIBs using this aqueous electrolyte exhibits a dramatically enhanced specific capacity, remarkable rate capability, and great cycling stability over a wide temperature range, from  $-50$  to  $25^{\circ}\text{C}$ . The aqueous ZIBs also exhibit an outstanding energy density of

Guoshen Yang, Jialei Huang, and Xuhao Wan contributed equally to this work.

This is an open access article under the terms of the Creative Commons Attribution License, which permits use, distribution and reproduction in any medium, provided the original work is properly cited.

© 2022 The Authors. *EcoMat* published by The Hong Kong Polytechnic University and John Wiley & Sons Australia, Ltd.

238.4 Wh/kg without compromising the power density (7.9 kW/kg) under  $-20^{\circ}\text{C}$ . Moreover, the assembled aqueous ZIBs can also cycle stably over 1000 cycles at an ultra-low  $-50^{\circ}\text{C}$ . The high-safety and cost-effective chaotropic salt electrolyte presented here is a promising strategy for low temperature energy storage application.

#### KEYWORDS

anti-freezing property, aqueous zinc ion batteries, high energy density, low-concentration aqueous electrolyte

## 1 | INTRODUCTION

With more and more renewable energy being exploited, it is urgent to develop high safety and environmental friendly energy storage devices to store electricity produced from renewable clean energy.<sup>1,2</sup> Rechargeable zinc-ion batteries (ZIBs) are promising technologies for large-scale energy storage due to the abundance of metal zinc, super safety, low redox potential ( $-0.76\text{ V}$  vs. the standard hydrogen electrode) and high theoretical capacity (820 mAh/g).<sup>3–6</sup> Moreover, ZIBs with aqueous electrolytes have the merits of high safety, low cost, and environmental friendliness. Unfortunately, at a low working temperature, the natural freeze of traditional aqueous electrolytes suffers from sharp drop in ionic conductivity, resulting in rapid deterioration of battery performance.<sup>7,8</sup> The freeze of aqueous electrolytes limits the further practicability of ZIBs in cold area or cold chain logistics. Consequently, it is a priority for restraining the electrolyte from freezing at subzero temperatures for constructing low-temperature aqueous ZIBs.

In fact, the freezing process of water involves the formation of hydrogen bonds (H-bonds) in ice crystals. To suppress the freeze of aqueous electrolyte, one effective strategy is to break the H-bonds network formed by water molecular. Up to now, the most adopted methods for lowering the freezing point of aqueous electrolytes include “water-in-salt” electrolyte<sup>9–11</sup> and adding organic cosolvents or anti-freezing additives in electrolyte.<sup>12–14</sup> For the former method, the highly concentrated electrolytes can significantly reduce the activity of free water molecules, thus decreasing the freezing point of the “water in-salt” electrolyte, which endows ZIBs to work at subzero temperatures. However, the high-concentration electrolytes also bring issues, such as high cost, high viscosity, and salt precipitation as the temperature dwindle. For the latter method, the addition of organic cosolvents or anti-freezing additives in electrolytes would weaken the environmental friendliness of aqueous electrolytes. Besides, the additional solvents or agents would add to the complexity of production and raise the cost of

the final electrolytes. To date, most frequently adopted five typical Zn-based aqueous electrolytes including  $\text{ZnSO}_4$ ,  $\text{ZnCl}_2$ ,  $\text{Zn}(\text{CF}_3\text{SO}_3)_2$ ,  $\text{Zn}(\text{CH}_3\text{COO})_2$ , and  $\text{Zn}(\text{NO}_3)_2$ , have been reported in ZIBs.<sup>3,15–18</sup> Unfortunately, the above electrolytes with the low concentrations are still suffering from the severe decline of ionic conductivity under subzero temperatures. Therefore, developing a low-concentration and organics solvent-free anti-freezing aqueous electrolyte with superior electrochemical performance is of importance for the practical application of aqueous ZIBs. Generally, the properties of anti-freezing aqueous electrolytes for the ZIBs shall possess the following features: (a) wide electrochemical window, (b) high ionic conductivity, and (c) good ability to withstand the low temperature condition.

Chaotropic salts, large monovalent ions with a low charge density, can effectively disrupt the network of hydrogen bonding of surrounding water due to the interaction between chaotropic salts and water molecules.<sup>19</sup> Apart from thiocyanate, perchlorate is the most chaotropic anion in the Hofmeister series.<sup>20</sup> In fact, it is found that the existence of liquid water in the ultra-low temperature environment of Martian is closely related to perchlorate.<sup>21</sup> Perchlorate is frequently used by scientists to obtain dehydrated macromolecules, such as DNA or proteins, that are saturated with hydrogen bonded  $\text{H}_2\text{O}$  molecules.<sup>22</sup> Due to the above facts, it is speculated that perchloric-based salt aqueous solution may possess good anti-freezing property and perchloric-based Zn salt could become an ideal aqueous electrolyte for constructing aqueous ZIBs with anti-freezing property. So far only Yan et al. reported that 1 M  $\text{Zn}(\text{ClO}_4)_2$  salty ice electrolyte enabled the as-built zinc-ion hybrid supercapacitor to achieve anti-freezing property.<sup>23</sup> Here, we further investigate this perchlorate-based chaotropic salt by modulating the electrolyte concentration and apply it to ZIBs. We discover that the 3 M  $\text{Zn}(\text{ClO}_4)_2$  aqueous electrolyte has optimum anti-freezing property, whose mechanism is different from previous reported salty ice electrolyte in zinc-ion hybrid supercapacitor. It is further confirmed

that zinc perchlorate electrolyte can be well compatible with electrode materials in ZIBs.

In this work, we formulated various concentrations of aqueous  $\text{Zn}(\text{ClO}_4)_2$ -based electrolytes without adding any organic cosolvents or anti-freezing additives. We discover that the 3 M  $\text{Zn}(\text{ClO}_4)_2$  aqueous exhibits a high ionic conductivity of 4.23 mS/cm at ultra-low  $-50^\circ\text{C}$ , proving its great anti-freezing capability. Through the experimental analysis and molecular dynamics (MD) simulations, it is found that the  $\text{Zn}(\text{ClO}_4)_2$  solution possess faster ionic migration than other Zn-based salts and can form more H-bonds between solute  $\text{ClO}_4^-$  and solvent  $\text{H}_2\text{O}$  which suppress the construction of ice crystals, resulting in a superior anti-freezing property. The assembled aqueous ZIBs device shows an outstanding energy density of 238.4 Wh/kg without compromising the power density (7.9 kW/kg) under  $-20^\circ\text{C}$ , which surpasses most previous ZIBs works. More significantly, the fabricated ZIBs still can stable charge/discharge at ultra-low  $-50^\circ\text{C}$  for 1000 cycles. The cost-effective, high-safety, and eco-friendly  $\text{Zn}(\text{ClO}_4)_2$  aqueous electrolytes have a promising practical application in aqueous ZIBs device working low temperature conditions.

## 2 | EXPERIMENTAL SECTION

### 2.1 | Chemical reagents

$\text{Zn}(\text{ClO}_4)_2 \cdot 6\text{H}_2\text{O}$  (AR, >99%),  $\text{ZnSO}_4 \cdot 7\text{H}_2\text{O}$  (AR, >99%), and  $\text{Zn}(\text{CF}_3\text{SO}_3)_2$  (AR, >99%) were purchased from Aladdin Chemical Reagent Co., Ltd..  $\text{MnSO}_4$  (AR, >99%) was purchased from Macklin Chemical Reagent Co., Ltd. rGO was purchased from China XFNANO Materials Tech Co., Ltd. Carbon cloth (wos1009) was purchased from CeTech Co., Ltd.

### 2.2 | Material preparation

*Preparation of  $\text{MnO}_2$  cathode and Zn anode:* The  $\alpha\text{-MnO}_2$  material was synthesized prepared using a hydrothermal method.<sup>24</sup> For the cathode slurry, 80 wt % of  $\alpha\text{-MnO}_2$ , 10 wt% of rGO, and 10 wt% of polyvinylidene fluoride (PVDF) were mixed in N-methyl pyrrolidone (NMP) under constant magnetic stirring for 6 h. Then, the slurry was spread onto carbon cloth and dried in oven at  $60^\circ\text{C}$  for 24 h. The mass loading of active materials ( $\alpha\text{-MnO}_2$ ) was about 1.5–2.0 mg. The Zn anode was carried out by a constant current electro-deposition technique in an aqueous medium (0.9 M  $\text{Na}_2\text{SO}_4$  + 0.4 M  $\text{ZnSO}_4 \cdot 7\text{H}_2\text{O}$  + 0.3 M  $\text{H}_3\text{BO}_3$ ). In electrochemical cell, a carbon cloth was used as the

working electrode and Pt plate was used as the counter/reference electrode. The  $-40 \text{ mA/cm}^2$  current density was applied for 15 min at room temperature. The mass loading of zinc was  $\sim 8 \text{ mg/cm}^2$  (The surface morphology of the as-prepared Zn is shown in Figure S1).

### 2.3 | Structural characterization and computational details

Fourier-transform infrared spectrometer and Raman spectrometer of electrolytes were collected through LabRAM HR800 (Horiba Jobin Yvon S.A.S) and Vertex-70 (Bruker). Differential scanning calorimetry measurement was examined by DSC1 (Mettler Toledo). The surface morphology of the samples was analyzed by field-emission scanning electron microscopy (SEM, Zeiss Supra, Carl Zeiss). Molecular dynamics simulation, called dynamic reaction coordinate (DRC) simulation, was carried out to investigate electrolytes by MOPAC 2016.<sup>25,26</sup> The integration time was 30 ns with a 1 fs interval and 1000 steps in total. The simulation temperature was 300 K. After 1 ps, the system was fully equilibrated, the data was collected for further analysis. The half-life ( $t_{1/2}$ ) for loss of kinetic energy is 50 fs. The model in this study was built and RDF (radial distribution function) was explored by using VMD3 (visual molecular dynamics). The electrolytes are surrounded by a  $[60 \times 60 \times 60] \text{ \AA}$  water box.<sup>27</sup>

### 2.4 | Assembly of aqueous ZIBs devices

Aqueous ZIBs devices were fabricated in CR2032 coin cell for cell performance evaluation by stacking the  $\alpha\text{-MnO}_2$  cathode, 50- $\mu\text{m}$  thick fiberglass separator (NKK-MPF30AC-100, Japan), 50  $\mu\text{L}$  electrolyte, and Zn anode. The electrolyte was obtained by dissolving different concentrations of  $\text{Zn}(\text{ClO}_4)_2 \cdot 6\text{H}_2\text{O}$  in pure water. The reported articles have proved that adding a small amount of  $\text{MnSO}_4$  could improve the cycle performance of ZIBs.<sup>24,28,29</sup> In the following experiments, if not specified, all electrolytes were added with 0.1 M manganese sulfate for further measurements. Besides,  $\text{ZnSO}_4$  and  $\text{Zn}(\text{CF}_3\text{SO}_3)_2$  were studied together with  $\text{Zn}(\text{ClO}_4)_2$  as the standard salt for aqueous zinc electrolytes.

### 2.5 | Electrochemical characterization

The linear sweep voltammetry (LSV), electrochemical impedance spectroscopy (EIS), and cyclic voltammetry (CV) were carried out on a CHI660 electrochemical

workstation (Shanghai CH Instrument Co., Ltd.). The electrochemical stability window was acquired via LSV, using stainless steel plate as working electrode, zinc foil as counter and reference electrode. The ionic conductivity was examined by EIS, frequency range was from 100 kHz to 0.01 Hz with an AC amplitude of 5 mV. The ion conductivity was calculated from the Nyquist plot using the following equations:

$$\sigma = \frac{L}{R_s A}$$

where  $\sigma$  (S/cm) represents the ion conductivity;  $A$  (cm<sup>2</sup>) is electrode contact area;  $L$  (cm) is interval distance between the two stainless steel electrodes;  $R_s$  ( $\Omega$ ) is the electrolyte resistance, which was obtained from the intercept with the  $x$ -axis in Nyquist plots. The rate performance and the cycling stability were carried out on a

Land CT2001A battery-test system (Wuhan Land Electronic Co., Ltd).

### 3 | RESULTS AND DISCUSSION

#### 3.1 | Characterization of the aqueous electrolytes

The low-temperature electrochemical performance of aqueous ZIBs is closely related to the freezing and ionic conductivity of the electrolyte at low temperature. As shown in Figure 1A, the Zn(ClO<sub>4</sub>)<sub>2</sub> aqueous solution with low concentration ( $\leq 2$  M) is frozen at  $-50^\circ\text{C}$ , while it becomes solid state again with the increase of solution concentration (5 M). As noted before, the freeze capability is mainly influenced by the H-bonds of free water. FTIR and Raman spectroscopy were performed to reflect

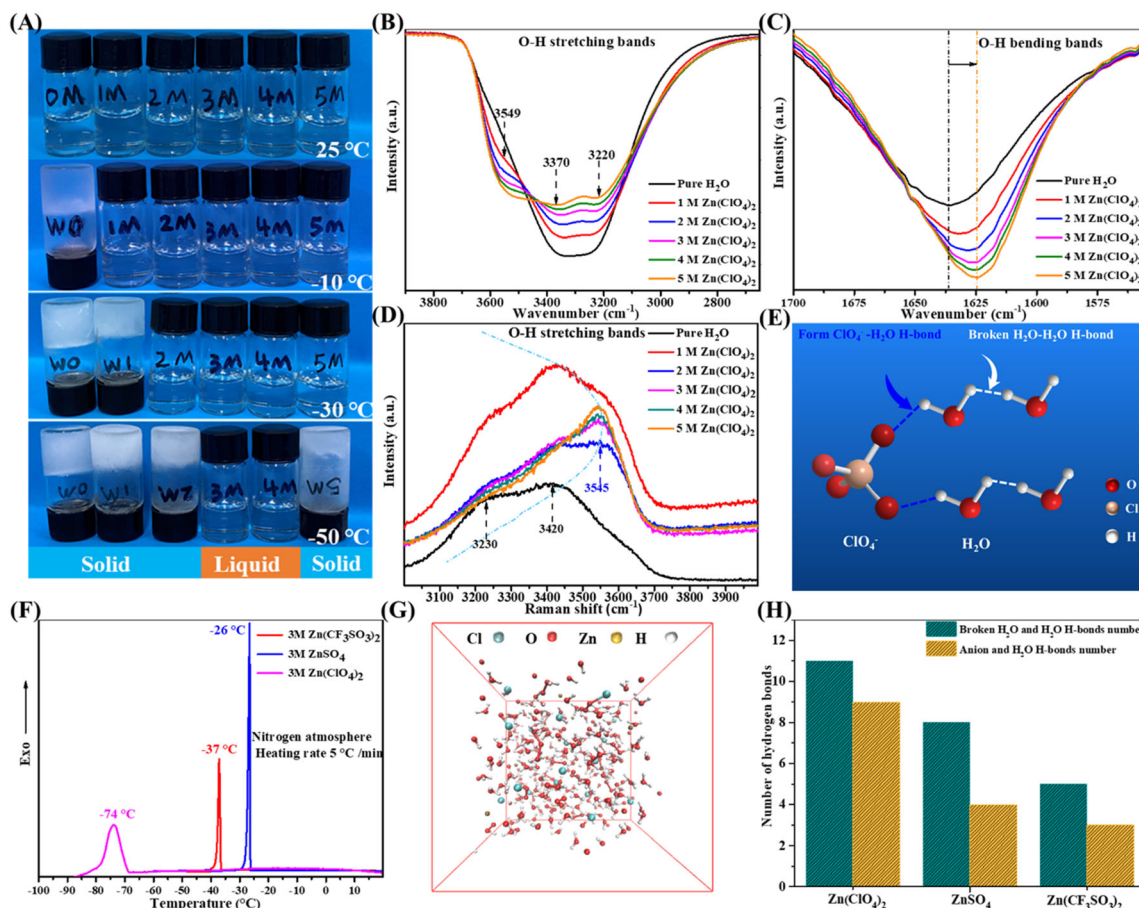


**FIGURE 1** Characterization of the aqueous solution: (A) The optical photographs of different concentration Zn(ClO<sub>4</sub>)<sub>2</sub> aqueous solution at 25,  $-10$ ,  $-30$ , and  $-50^\circ\text{C}$ . (B, C) FTIR spectrum of pure H<sub>2</sub>O and the Zn(ClO<sub>4</sub>)<sub>2</sub> aqueous solutions with various concentration, showing the O–H stretching band and the O–H bending band, respectively. (D) Raman spectrum of pure H<sub>2</sub>O and the Zn(ClO<sub>4</sub>)<sub>2</sub> aqueous solution with various concentration. (E) Schematic illustration of a possible mechanism of how the perchlorate anions interaction impacts the H-bonds of the Zn(ClO<sub>4</sub>)<sub>2</sub> aqueous solution. (F) DSC curves of 3 M ZnSO<sub>4</sub>, 3 M Zn(CF<sub>3</sub>SO<sub>3</sub>)<sub>2</sub>, and 3 M Zn(ClO<sub>4</sub>)<sub>2</sub>. (G) The snapshot of the MD simulation of Zn(ClO<sub>4</sub>)<sub>2</sub> aqueous solution. (H) Averaged hydrogen bonds numbers for Zn(ClO<sub>4</sub>)<sub>2</sub>, ZnSO<sub>4</sub>, and Zn(CF<sub>3</sub>SO<sub>3</sub>)<sub>2</sub> systems. (A color version of this figure can be viewed online)

the H-bonds changes in  $\text{Zn}(\text{ClO}_4)_2$  aqueous solution with the increasing concentration. As displayed in Figure 1B, there are a main peak at  $3370\text{ cm}^{-1}$  and two shoulders at  $3220$  and  $3549\text{ cm}^{-1}$ , owing to the O–H stretching bands. For the pure water, the peak at  $1637\text{ cm}^{-1}$  belongs to O–H bending bands in Figure 1C. It is observed that the O–H bending bands shift from  $1637$  to  $1624\text{ cm}^{-1}$  with increasing the concentration of  $\text{Zn}(\text{ClO}_4)_2$ . Furthermore, with increasing concentration, the low wavenumber  $3220\text{ cm}^{-1}$  shoulder decreases and the high wavenumber  $3549\text{ cm}^{-1}$  shoulder increases. This phenomenon is in consistent with previous reported “structure breaking” effect of solute  $\text{ClO}_4^-$  anion on the H-bonds network of solvent  $\text{H}_2\text{O}$ .<sup>30,31</sup> In Raman spectrum (Figure 1D), it has an O–H stretching envelope between  $3000$  and  $3700\text{ cm}^{-1}$ , where the band at  $\sim 3230\text{ cm}^{-1}$  stands for the ice-like component, the band at  $\sim 3420\text{ cm}^{-1}$  is the ice-like liquid component, and the band at  $\sim 3530\text{ cm}^{-1}$  represents the liquid-like amorphous phase.<sup>32</sup> The two bands at lower wavenumbers are responsible for the H-bonded free water molecules.<sup>33</sup> The new band in  $\text{Zn}(\text{ClO}_4)_2$  solutions at  $\sim 3545\text{ cm}^{-1}$  represents the water molecules coordinated anions with H-bonds.<sup>34,35</sup> When the concentration of  $\text{Zn}(\text{ClO}_4)_2$  increase, two lower bands at  $3230$  and  $3420\text{ cm}^{-1}$  strongly decreases. For instance, in  $3\text{ M Zn}(\text{ClO}_4)_2$  solution, the band at  $3230\text{ cm}^{-1}$  almost disappear and the band at  $3420\text{ cm}^{-1}$  is hardly observed, which means that the H-bonds of free water molecules were broken. Moreover, the Cl–O stretching ( $\sim 936\text{ cm}^{-1}$ ) of  $\text{ClO}_4^-$  gradually strengthens following the concentration increase, which discloses that it forms strong H-bonded interactions between  $\text{ClO}_4^-$  and water, but the rising trend is limited when the concentration is greater than  $3\text{ M}$  (Figure S2). This phenomenon was also found in recently reported  $\text{H}_2\text{SO}_4$  work.<sup>36</sup> Together with FTIR results, it suggests that the H-bonds are seriously destructed with increasing the concentration, and the strong H-bonded interaction is formed between  $\text{ClO}_4^-$  and water molecules, therefore suppressing the establishment of ice crystals and lowering the freeze points (Figure 1E). In order to help the reader to understand the anti-freezing property of  $\text{Zn}(\text{ClO}_4)_2$ , the differential scanning calorimetry (DSC) measurements were carried out to observe freezing points of three typical different zinc salt electrolyte with  $3\text{ M}$  concentration. As shown in Figure 1F, the freezing points of  $\text{ZnSO}_4$ ,  $\text{Zn}(\text{CF}_3\text{SO}_3)_2$ , and  $\text{Zn}(\text{ClO}_4)_2$  are  $-26$ ,  $-37$ , and  $-74^\circ\text{C}$ , respectively.

To further explore the effect of the low-temperature mechanism of  $\text{Zn}(\text{ClO}_4)_2$  aqueous solution, MD simulations were performed (Figure 1G) with  $\text{ZnSO}_4$  and  $\text{Zn}(\text{CF}_3\text{SO}_3)_2$  aqueous solution simulated at the same condition for comparison (Figure S3A,B). Conformation analysis for the  $\text{Zn}(\text{ClO}_4)_2$  system is presented in

Figure 1G. Normally, in aqueous electrolytes, strong H-bonds form between free water molecules.<sup>4</sup> Each water molecule can combine the other four water molecules via H-bonds, forming a tetrahedral H-bond structure, where it keeps dynamic balance between breaking and recombining. When the temperature drops under the freezing point, H-bonds form more quickly and they break the balance and cause the formation of ice crystals.<sup>37,38</sup> Therefore, one effective way to break the original H-bond network is by introducing ions to form stronger H-bonded interaction with water molecules. The number change of H-bonds between anions- $\text{H}_2\text{O}$  and  $\text{H}_2\text{O}$ - $\text{H}_2\text{O}$  molecules are exhibited in Figure 1H. By statistic analysis, the number of H-bonds formed in anions- $\text{H}_2\text{O}$  is 4 in  $3\text{ M ZnSO}_4$  and 3 in  $3\text{ M Zn}(\text{CF}_3\text{SO}_3)_2$ , while the number of H-bonds formed in  $\text{ClO}_4^-$ - $\text{H}_2\text{O}$  can increase to 9 in  $3\text{ M Zn}(\text{ClO}_4)_2$ . The results indicated that the  $\text{ClO}_4^-$  anions can more effective forms H-bonds with water molecule comparing with other two electrolytes. In addition, the formation of new H-bonds between anions and  $\text{H}_2\text{O}$  molecules is accompanied by the breaking of H-bonds between  $\text{H}_2\text{O}$  molecules. According to previous studies,<sup>20,39</sup> the effect of ions on the structure of water usually follows the Hofmeister sequence. As shown in Figure S3C, the ions on the left are classified as “structuring making,” strengthening H-bonds network of free water. The ions on the right of Figure S3C have the reverse effect, classified as “structuring breaking,” which help break the H-bonds network of free water. In this way, the dynamic balance can be rebuilt via new H-bonded interactions between  $\text{ClO}_4^-$  and water molecules, thus leading to lower freezing points. Altogether, the results of simulations are also consistent with above characterizations, proving the great anti-freezing performance of the  $\text{Zn}(\text{ClO}_4)_2$  electrolyte system.

The ionic conductivity of  $\text{Zn}(\text{ClO}_4)_2$  aqueous solution with various concentration was further studied under different temperatures by calculating through EIS data (Figure S4) and the values of ionic conductivity are displayed in Figure 2A. As shown in Figure 2A, it displays an increase of ionic conductivity in the  $\text{Zn}(\text{ClO}_4)_2$  electrolyte with increasing electrolyte concentration until it reaches its maximum at  $3\text{ M}$ . Further increasing the concentration would lead to reduction of the ionic conductivity. It is probably due to the strengthened interactions between cations and anions, which brings about high viscosity, leading to a detrimental process of mass transfer.<sup>36</sup> For the same concentration, the ionic conductivities of  $\text{Zn}(\text{ClO}_4)_2$  show a downward trend as the temperature decreases from  $25$  to  $-50^\circ\text{C}$ . Notably, the  $3\text{ M Zn}(\text{ClO}_4)_2$  aqueous solution has the highest ionic conductivity within the whole temperature range, and it can still maintain a value  $4.23\text{ mS/cm}$  even at ultra-low  $-50^\circ\text{C}$ ,

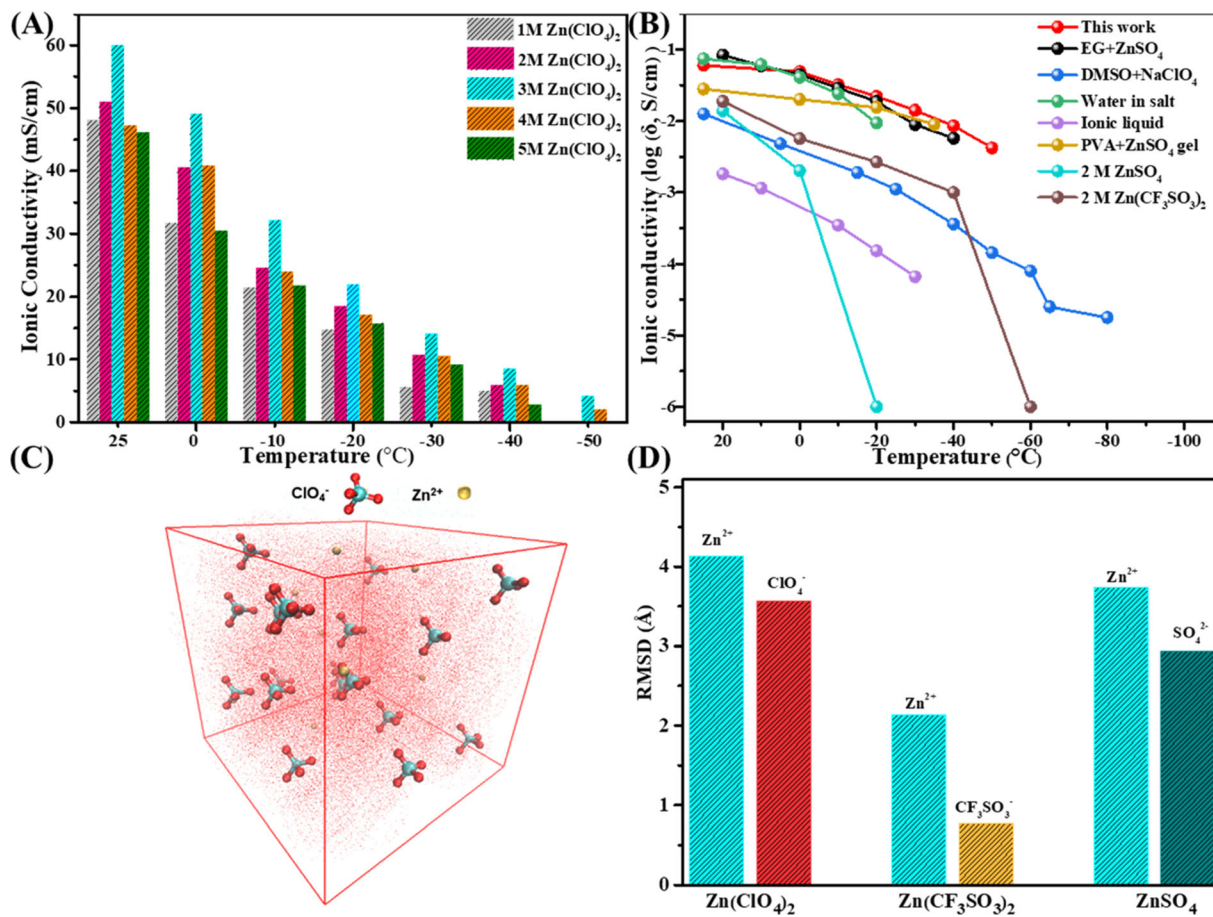


**FIGURE 2** (A) Ionic conductivity comparisons of the aqueous Zn(ClO<sub>4</sub>)<sub>2</sub> aqueous solution with various concentration under different temperatures. (B) Comparison of the 3 M Zn(ClO<sub>4</sub>)<sub>2</sub> aqueous solution with various other low-temperature electrolytes. (C) Molecular dynamics simulation snapshot of Zn(ClO<sub>4</sub>)<sub>2</sub> aqueous solution. (D) Root mean square deviation values of Zn(ClO<sub>4</sub>)<sub>2</sub>, ZnSO<sub>4</sub>, and Zn(CF<sub>3</sub>SO<sub>3</sub>)<sub>2</sub>, respectively

justifying its highest anti-freezing capability. Thus, the 3 M Zn(ClO<sub>4</sub>)<sub>2</sub> with the optimal ionic conductivity was selected as the electrolyte for aqueous ZIBs in this work. Surprisingly, the as-prepared 3 M Zn(ClO<sub>4</sub>)<sub>2</sub> aqueous solution also exhibits one of the highest ionic conductivities comparing with recently reported electrolytes at low temperatures (Figure 2B).<sup>12,40–42</sup> Likewise, 3 M Zn(ClO<sub>4</sub>)<sub>2</sub> aqueous solution as electrolytes provides a good balance between cost and low temperature performance, which enables promising energy storage in low temperature conditions.

Furthermore, a preliminary analysis combining with simulations was conducted to elucidate the excellent ionic conductivity in Zn(ClO<sub>4</sub>)<sub>2</sub>. Figure 2C and Figure S5A,B exhibit the snapshots of the simulated electrolyte structure. It shows the ionic clusters of Zn<sup>2+</sup> coordinating with ClO<sub>4</sub><sup>-</sup>, CF<sub>3</sub>SO<sub>3</sub><sup>-</sup>, SO<sub>4</sub><sup>2-</sup>, and H<sub>2</sub>O in corresponding aqueous electrolytes. The root mean square displacement (RMSD) can reflect the ion diffusion properties of electrolytes (Figure 2D). Specifically, RMSD

values represent the ions' diffusion distances of the electrolyte as compared to their starting point. After 20 ns dynamics runs, the anion RMSD values of Zn(ClO<sub>4</sub>)<sub>2</sub>, Zn(CF<sub>3</sub>SO<sub>3</sub>)<sub>2</sub>, and ZnSO<sub>4</sub> are 3.56, 0.78, and 2.94 Å, and the cation RMSD values of them are 4.13, 2.13, and 3.73 Å, respectively. The higher RMSD values in Zn(ClO<sub>4</sub>)<sub>2</sub> electrolyte suggest that the ions diffusion in Zn(ClO<sub>4</sub>)<sub>2</sub> electrolyte is more favorable than that of ZnSO<sub>4</sub> and Zn(CF<sub>3</sub>SO<sub>3</sub>)<sub>2</sub> electrolyte. Overall, our MD simulation confirms that Zn(ClO<sub>4</sub>)<sub>2</sub> system has higher diffusion coefficient, thus leading to the faster ion migration, which can effectively accelerate the electrochemical reaction in aqueous ZIBs.

### 3.2 | Electrochemical performance of aqueous ZIBs device

To evaluate the electrochemical performance of the as-prepared electrolyte, an aqueous α-MnO<sub>2</sub>//Zn device was

fabricated with 3 M  $\text{Zn}(\text{ClO}_4)_2$  electrolyte, as illustrated in Figure 3A. It has been proved that adding a small amount of  $\text{MnSO}_4$  in electrolyte could suppress the dissolution of  $\text{MnO}_2$  and improve the cycle performance of ZIBs (see Figure S6).<sup>24,28,29</sup> We therefore used the mixture solution of 3 M  $\text{Zn}(\text{ClO}_4)_2 + 0.1$  M  $\text{MnSO}_4$  (labeled as ZCM) as electrolyte to assemble ZIBs. For comparison, 3 M  $\text{Zn}(\text{CF}_3\text{SO}_3)_2 + 0.1$  M  $\text{MnSO}_4$  (denoted as ZFM) and

3 M  $\text{ZnSO}_4 + 0.1$  M  $\text{MnSO}_4$  (labeled as ZSM) electrolytes were also applied in ZIBs. Firstly, the electrochemical stability window of electrolytes was verified by applying LSV measurement. As shown in Figure 3B, the oxidative onset potentials are  $\sim 2.2$  V in 3 M ZSM and  $\sim 2.3$  V in 3 M ZFM, while the onset potential can be pushed to  $\sim 2.5$  V in 3 M ZCM. Following reported works, the suitable potential window of aqueous  $\text{MnO}_2$ -Zn ZIBs is about 1.0–

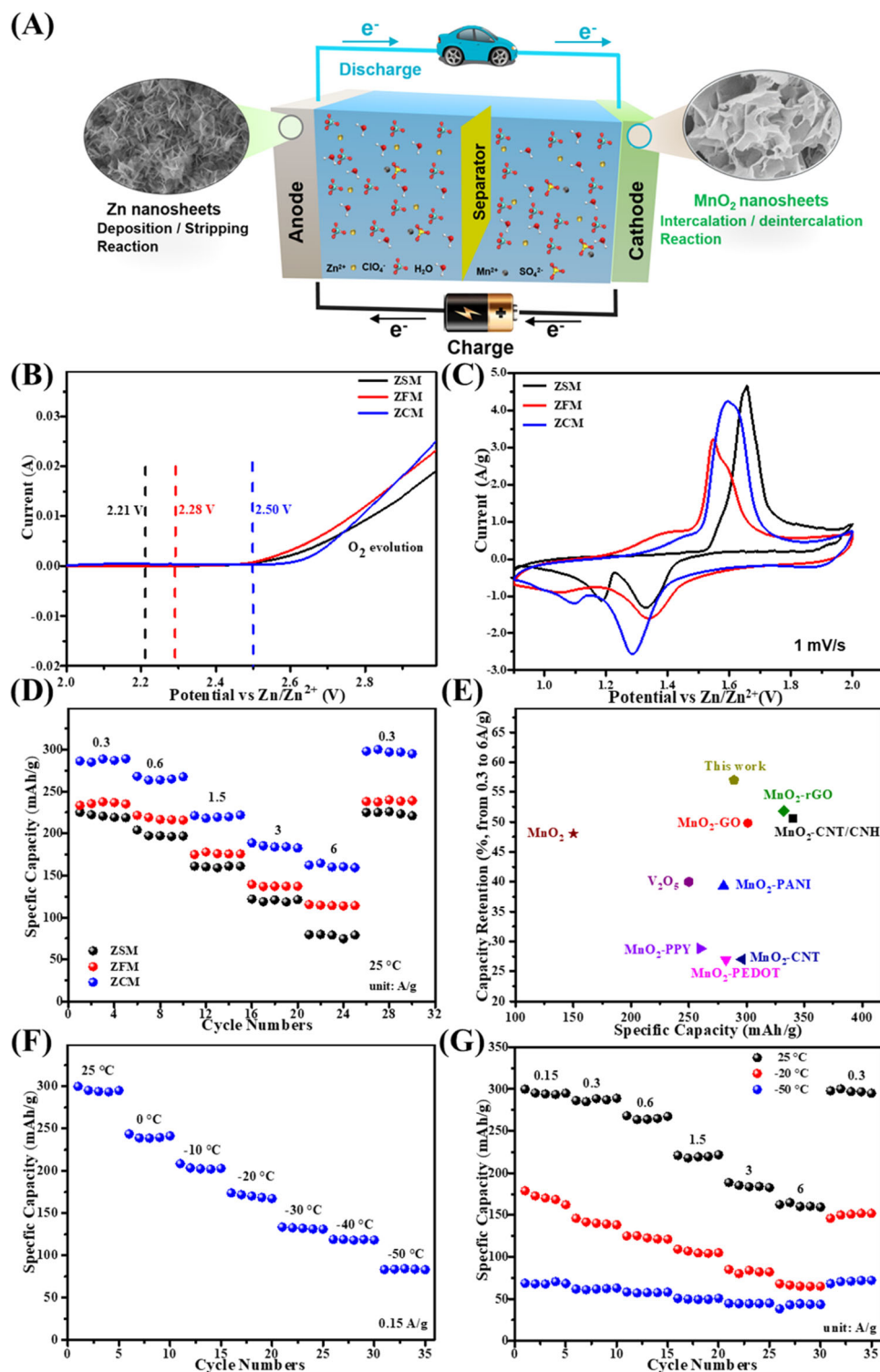


**FIGURE 3** Electrochemical performance of aqueous ZIBs device. (A) Schematic illustration of the  $\alpha\text{-MnO}_2//\text{ZCM (aq.)//Zn}$  device. (B) LSV curves of the electrochemical stability window of 3 M ZCM, 3 M ZFM, and 3 M ZSM. (C) CV curves and (D) Rate performance of aqueous ZIBs device with different electrolytes at room temperature. (E) Balance relationship between capacity retentions and specific capacities for different aqueous ZIBs.<sup>18,24,43–49</sup> (F) Specific capacities at different temperature of aqueous ZIBs device with 3 M ZCM at 0.15 A/g. (G) Specific capacities with various current density of ZIBs device with 3 M ZCM electrolytes at 25,  $-20$ , and  $-50$  °C



1.9 V.<sup>24,50</sup> The enlarged potential range in 3 M ZCM is capable to perform almost all aqueous ZIBs devices. Figure 3C displays the CV curves at 1 mV/s of corresponding ZIBs with different electrolytes. All the aqueous ZIBs display a single oxidation peak (~1.6 V) and two reduction peaks (~1.1 V and ~1.3 V) in the CV curves, corresponding to a two-step reaction during charging–discharging process. Specifically, over the discharging process, the zinc ions insert in  $\alpha\text{-MnO}_2$  at ~1.3 V, and then a proton conversion reaction occurs around 1.1–1.3 V.<sup>51</sup> Notably,  $\alpha\text{-MnO}_2//\text{ZCM (aq.)//Zn}$  has the largest enclosed area, indicating a higher capacity.<sup>44,52</sup> Figure 3D shows the rate performances of ZIBs with ZSM, ZFM, and ZCM electrolytes at room temperature. By calculation, the specific capacity of  $\alpha\text{-MnO}_2//\text{ZSM (aq.)//Zn}$ ,  $\alpha\text{-MnO}_2//\text{ZFM (aq.)//Zn}$ , and  $\alpha\text{-MnO}_2//\text{ZCM (aq.)//Zn}$  are 220.7, 237.7, and 289 mAh/g at 0.3 A/g and the specific capacity retentions of them are 35%, 44%, and 57% at 6 A/g, respectively (Figure 3D). When the current density returns to 0.3 A/g, the discharge capacity of  $\alpha\text{-MnO}_2//\text{ZCM (aq.)//Zn}$  can reach 301 mAh/g. The  $\alpha\text{-MnO}_2//\text{ZCM (aq.)//Zn}$  displays the greatest specific capacity performance and rate capability compared with those of  $\alpha\text{-MnO}_2//\text{ZSM (aq.)//Zn}$  and  $\alpha\text{-MnO}_2//\text{ZFM (aq.)//Zn}$ . Moreover, as shown in Figure 3E, the prominent rate performance of  $\alpha\text{-MnO}_2//\text{ZCM (aq.)//Zn}$  already surpasses many previously reported ZIBs devices (see Table S1 for details).<sup>18,24,43–49</sup> It is worth to note that this is achieved only due to the use of ZCM electrolyte and without any chemical modification of electrode material.

The operating temperature range is a critical parameter for energy storage devices, especially for the device working in low temperatures environments. We also further evaluated the low temperature performance of the ZCM electrolytes. Figure S7 displays CV curves of ZCM electrolytes under various temperatures at 1 mV/s. The intensity of peak current decreases as the temperature decrease, indicating the reducing capacity. Meanwhile, the proton conversion reaction peak disappeared when the temperature drops below zero, which is further confirmed by the charge/discharge curves (Figure S8). Figure 3F shows the discharge capacities in the ZCM electrolyte under various temperatures at 0.15 A/g. The aqueous ZIBs display around 295 mAh/g at 25°C. The aqueous ZIBs still has approximate 170 mAh/g at –20°C, which is almost 58% capacity retention compared to that at 25°C. More significantly, from 25 to ultra-low –50°C, the ZIBs can still keep a high-capacity retention of 29%. It is worth to note that this good performance is achieved without adding any other anti-freezing agent. To further highlight the anti-freezing capability of the aqueous ZIBs with ZCM electrolytes, the rate capabilities at –20 and

–50°C were also measured by increasing the current density from 0.15 to 6 A/g gradually (Figure 3G). At the low temperature –20°C, the aqueous ZIBs delivered a discharging capacity of ~175 mAh/g at 0.15 A/g and ~69 mAh/g at 6 A/g, which is almost 40% capacity retention. At the ultra-low –50°C, the aqueous ZIBs delivers a discharging capacity of ~69 mAh/g at 0.15 A/g and ~44 mAh/g at 6 A/g, which is almost 64% capacity retention. When the current density returned to 0.15 A/g, the capacity slightly increases. The results indicate that the great capacity and rate performance of this aqueous ZIBs working at low temperatures, and it also strongly prove the impressive anti-freezing property of low concentration ZCM electrolytes.

Electrochemical impedance spectroscopy measurement was employed to further explore the electrochemical behavior of the ZIBs with varying working temperatures, and the Nyquist plots are shown in Figure 4A. In the Nyquist plot, the equivalent serial internal resistance ( $R_s$ ) is the intercept with the real part in the high frequency region and charge-transfer resistance ( $R_{ct}$ ) is the diameter of semicircle. The inset in Figure 4A is the equivalent circuit model, and the relative parameters are summarized in Table S2. With decreasing the ambient temperature from 25 to –40°C, the  $R_s$  and  $R_{ct}$  show an increasing tendency. It is highlighted that the electrolyte has a strong effect on the electrochemical performance. With the decrease of working temperature, the ion mobility of aqueous ZCM electrolyte decreases, which leads to the decrease of ionic conductivity. The reduced ionic conductivity caused the increase of  $R_s$ . The kinetics of active materials for  $\text{Zn}^{2+}$  ions de/intercalation decrease significantly with reducing temperature, which will result in an increased  $R_{ct}$ . The cycling stability of the ZIBs device was evaluated by the charge/discharge process at a high current density of 6 A/g. As shown in Figure 4B, over 1000 cycles, the specific capacity retentions of ZIBs are almost 100% at 25°C. Significantly, the cycling durability was achieved under –20 and ultra-low –50°C, which continuously operated over 1000 cycles without noticeable capacity decay. The results of cycling stability uncover that the aqueous ZIBs device is able to charge/discharge stably under a room temperature and even ultra-low temperature. Ragone plots can evaluate the ZIBs device's output in terms of energy and power density. Remarkably, our ZIBs device delivers an outstanding energy density of 238.4 Wh/kg and a power density of 7.9 kW/kg under –20°C (Figure 4C), which is significantly superior to previous reported ZIBs devices working under low temperatures condition.<sup>4,12,53–58</sup> Note that these values were obtained based on the loading mass of  $\text{MnO}_2$  cathode. To verify its practical application, the assembled aqueous ZIBs device was used to light an electric desktop

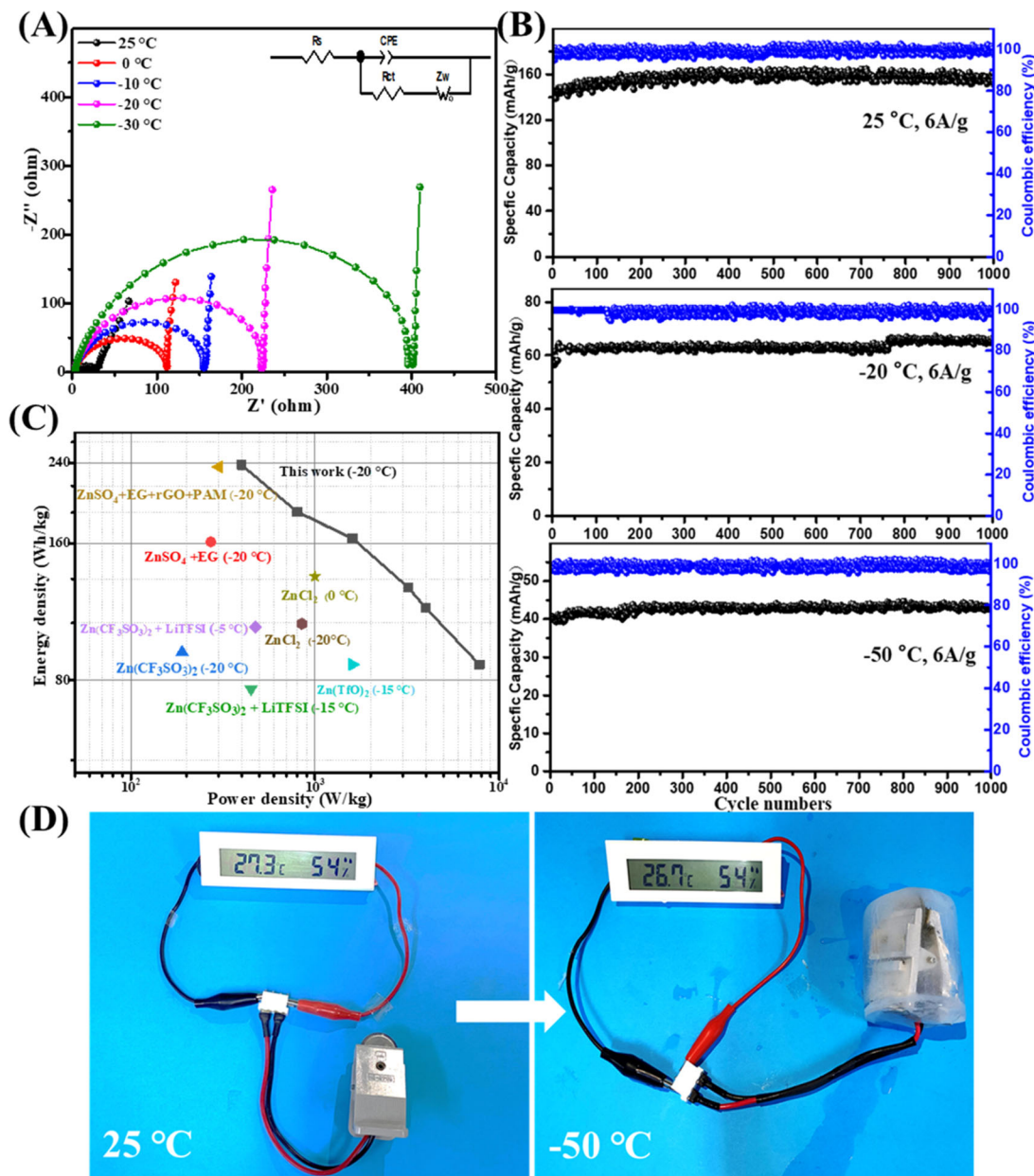


**FIGURE 4** (A) Nyquist plots of aqueous ZIBs device with 3 M  $\text{Zn}(\text{ClO}_4)_2$  at different temperature. (B) Cycling performance of aqueous ZIBs device at different temperatures. (C) Ragone plot of  $\text{MnO}_2//\text{ZCM}(\text{aq})//\text{Zn}$  device in comparison to other ZIBs at  $-20^\circ\text{C}$ . (D) Digital photographs of powered digital watch by the aqueous ZIBs at 25 and  $-50^\circ\text{C}$

clock after being charged to 1.9 V at  $25^\circ\text{C}$  and  $-50^\circ\text{C}$ , indicating our new assembled ZIBs with ZCM electrolytes has a considerable potential in practical renewable energy storage working within a wide temperature range (Figure 4D, Video S1, and Video S2).

## 4 | CONCLUSIONS

In this work, a cost-effective, anti-freezing, and high ionic conductivity  $\text{Zn}(\text{ClO}_4)_2$  electrolyte is discovered and applied in low-temperature aqueous ZIBs. The 3 M

$\text{Zn}(\text{ClO}_4)_2$  aqueous solution without adding any organic additives exhibit a high ionic conductivity of 4.23 mS/cm at even ultra-low  $-50^\circ\text{C}$ . Spectroscopic characterization and MD simulations revealed that the H-bond among free water was destructed and the new H-bonded interaction between  $\text{ClO}_4^-$  and water molecules generated, and the  $\text{Zn}(\text{ClO}_4)_2$  possesses faster ionic migration and it has more new H-bonds compared to other Zn-based salts, thereby leading to a superior anti-freezing property. As a result, the assembled aqueous ZIBs device using 3 M  $\text{Zn}(\text{ClO}_4)_2$  electrolyte displays a dramatically improved specific capacity, excellent rate capability, and superior

cycling stability under a wide temperature range, from  $-50$  to  $25^{\circ}\text{C}$ . The aqueous ZIBs also exhibit an outstanding energy density of  $238.4\text{ Wh/kg}$  with a power density of  $7.9\text{ kW/kg}$  under  $-20^{\circ}\text{C}$ . In this work, we not only propose a first reporting cost-effective, high-safety, anti-freezing, and eco-friendly  $\text{Zn}(\text{ClO}_4)_2$  aqueous electrolyte exerting great electrochemical performance in ZIBs devices, but also shows the deep understanding of effects on freeze points by anions, which exhibits the potential commercial applications for energy storage under low temperatures.

## ACKNOWLEDGMENTS

This work is supported by Shenzhen Science and Technology Innovation Committee (Nos. JCYJ20190806145609284, GJHZ20190820091203667, JSGG20201102161000002), Guangdong Basic and Applied Basic Research Foundation (2020A1515010716), and the Guangdong Introducing Innovative and Entrepreneurial Teams Program (2019ZT08Z656). P.H. would like to acknowledge Shenzhen Science and Technology Program (KQTD20190929172522248).

## CONFLICT OF INTEREST

The authors declare no conflict of interest.

## ORCID

Hang Zhou  <https://orcid.org/0000-0002-0472-9515>

## REFERENCES

- Armand M, Tarascon J. Building better batteries. *Nature*. 2008; 451(7179):652-657.
- Chao D, Zhou W, Xie F, et al. Roadmap for advanced aqueous batteries: from design of materials to applications. *Sci Adv*. 2020;6(21):eaba4098.
- Xu C, Li B, Du H, et al. Energetic zinc ion chemistry: the rechargeable zinc ion battery. *Angew Chem Int Ed*. 2012;51(4):933-935.
- Chao D, Zhou W, Ye C, et al. An electrolytic Zn–MnO<sub>2</sub> battery for high-voltage and scalable energy storage. *Angew Chem Int Ed*. 2019;58(23):7823-7828.
- Chao D, Qiao S. Toward high-voltage aqueous batteries: super- or low-concentrated electrolyte? *Joule*. 2020;4(9):1846-1851.
- Huang Y, Zhang J, Liu J, et al. Flexible and stable quasi-solid-state zinc ion battery with conductive guar gum electrolyte. *Mater Today Energy*. 2019;14:100349.
- Sun Y, Ma P, Liu L, et al. Solar-thermal driven self-heating of micro-supercapacitors at low temperatures. *Sol RRL*. 2018;2(12):1800223.
- Zhu M, Wang X, Tang H, et al. Antifreezing hydrogel with high zinc reversibility for flexible and durable aqueous batteries by cooperative hydrated cations. *Adv Funct Mater*. 2020;30(6):1907218.
- Zhao Y, Chen Z, Mo F, et al. Aqueous rechargeable metal-ion batteries working at subzero temperatures. *Adv Sci*. 2021;8(1):2002590.
- Chao D, Ye C, Xie F, et al. Atomic engineering catalyzed MnO<sub>2</sub> electrolysis kinetics for a hybrid aqueous battery with high power and energy density. *Adv Mater*. 2020;32(25):2001894.
- Reber D, Kühnel RS, Battaglia C. Suppressing crystallization of water-in-salt electrolytes by asymmetric anions enables low-temperature operation of high-voltage aqueous batteries. *ACS Mater Lett*. 2019;1(1):44-51.
- Chang N, Li T, Li R, et al. An aqueous hybrid electrolyte for low-temperature zinc-based energy storage devices. *Energ Environ Sci*. 2020;13(10):3527-3535.
- Yang W, Du X, Zhao J, et al. Hydrated eutectic electrolytes with ligand-oriented solvation shells for long-cycling zinc-organic batteries. *Joule*. 2020;4(7):1557-1574.
- Wu S, Alsaid Y, Yao B, et al. Rapid and scalable fabrication of ultra-stretchable, anti-freezing conductive gels by cononsolvency effect. *EcoMat*. 2021;3(2):e12085.
- Han S, Rajput N, Qu X, et al. Origin of electrochemical, structural, and transport properties in nonaqueous zinc electrolytes. *ACS Appl Mater Interfaces*. 2016;8(5):3021-3031.
- Jayachandran M, Rose A, Maiyalagan T, et al. Effect of various aqueous electrolytes on the electrochemical performance of  $\alpha\text{-MnO}_2$  nanorods as electrode materials for supercapacitor application. *Electrochim Acta*. 2021;366:137412.
- Pan H, Ellis J, Li X, et al. Electrolyte effect on the electrochemical performance of mild aqueous zinc-electrolytic manganese dioxide batteries. *ACS Appl Mater Interfaces*. 2019;11(41):37524-37530.
- Zhang N, Cheng F, Liu Y, et al. Cation-deficient spinel ZnMn<sub>2</sub>O<sub>4</sub> cathode in Zn(CF<sub>3</sub>SO<sub>3</sub>)<sub>2</sub> electrolyte for rechargeable aqueous Zn-ion battery. *J Am Chem Soc*. 2016;138(39):12894-12901.
- Koontz L. Chapter two-explanatory chapter: how plasmid preparation kits work. *Methods Enzymol*. Elsevier Academic Press INC. 2013;529:23-28.
- Zhang Y, Cremer P. Interactions between macromolecules and ions: the Hofmeister series. *Curr Opin Chem Biol*. 2006;10(6):658-663.
- Hecht M, Kounaves S, Quinn R, et al. Detection of perchlorate and the soluble chemistry of Martian soil at the Phoenix Lander site. *Science*. 2009;325(5936):64-67.
- Nieszporek K, Nieszporek J. Multi-centred hydrogen bonds between water and perchlorate anion. *Phys Chem Liq*. 2017;55(4):473-481.
- Sun Y, Ma H, Zhang X, et al. Salty ice electrolyte with superior ionic conductivity towards low-temperature aqueous zinc ion hybrid capacitors. *Adv Funct Mater*. 2021;31(28):2101277.
- Huang Y, Liu J, Huang Q, et al. Flexible high energy density zinc-ion batteries enabled by binder-free MnO<sub>2</sub>/reduced graphene oxide electrode. *NPJ Flex Electron*. 2018;2(1):21.
- Stewart JJ. MOPAC: a semiempirical molecular orbital program. *J Comput Aided Mol Des*. 1990;4(1):1-103.
- Dieter KM, Stewart JJP. Calculation of vibrational frequencies using molecular trajectories. *J. Mol. Struct. Theochem*. 1988;40:143-149.
- Humphrey W, Dalke A, Schulten K. VMD: visual molecular dynamics. *J Mol Graph*. 1996;14(1):33-38.
- Pan H, Shao Y, Yan P, et al. Reversible aqueous zinc/manganese oxide energy storage from conversion reactions. *Nat Energy*. 2016;1:16039.
- Zhang N, Cheng F, Liu J, et al. Rechargeable aqueous zinc-manganese dioxide batteries with high energy and power densities. *Nat Commun*. 2017;8(1):1-9.
- Chen Y, Zhang Y-H, Zhao L-J. ATR-FTIR spectroscopic studies on aqueous LiClO<sub>4</sub>, NaClO<sub>4</sub>, and Mg(ClO<sub>4</sub>)<sub>2</sub> solutions. *Phys Chem Chem Phys*. 2004;6(3):537-542.

31. Walrafen GE. Raman spectral studies of the effects of perchlorate ion on water structure. *J Chem Phys.* 1970;52(8):4176-4198.
32. Bu X, Su L, Dou Q, et al. A low-cost "water-in-salt" electrolyte for a 2.3 V high-rate carbon-based supercapacitor. *J Mater Chem A.* 2019;7(13):7541-7547.
33. Zhang Y-H, Chan CK. Observations of water monomers in supersaturated NaClO<sub>4</sub>, LiClO<sub>4</sub>, and Mg(ClO<sub>4</sub>)<sub>2</sub> droplets using Raman spectroscopy. *J Phys Chem A.* 2003;107(31):5956-5962.
34. Yamada Y, Usui K, Sodeyama K, et al. Hydrate-melt electrolytes for high-energy-density aqueous batteries. *Nat Energy.* 2016;1:16129.
35. Zhang Y-H, Chan CK. Understanding the hygroscopic properties of supersaturated droplets of metal and ammonium sulfate solutions using Raman spectroscopy. *J Phys Chem A.* 2002;106(2):285-292.
36. Yue F, Tie Z, Deng S, et al. An ultralow temperature aqueous battery with proton chemistry. *Angew Chem Int Ed.* 2021;60(25):13882-13886.
37. Sun CQ, Zhang X, Fu X, et al. Density and phonon-stiffness anomalies of water and ice in the full temperature range. *J Phys Chem Lett.* 2013;4(19):3238-3244.
38. Ma L, Chen S, Li N, et al. Hydrogen-free and dendrite-free all-solid-state Zn-ion batteries. *Adv Mater.* 2020;32(14):1908121.
39. Zhang Y, Cremer PS. Chemistry of Hofmeister anions and osmolytes. *Rev Phys Chem.* Annual Reviews. 2010;61:63-83.
40. Nian Q, Wang J, Liu S, et al. Aqueous batteries operated at -50°C. *Angew Chem Int Ed.* 2019;58(47):16994-16999.
41. Eftekhari A. Low voltage anode materials for lithium-ion batteries. *Energy Stor Mater.* 2017;7:157-180.
42. Chen M, Zhou W, Wang A, et al. Anti-freezing flexible aqueous Zn-MnO<sub>2</sub> batteries working at -35°C enabled by a borax-crosslinked polyvinyl alcohol/glycerol gel electrolyte. *J Mater Chem A.* 2020;8(14):6828-6841.
43. Wang C, Zeng Y, Xiao X, et al.  $\gamma$ -MnO<sub>2</sub> nanorods/graphene composite as efficient cathode for advanced rechargeable aqueous zinc-ion battery. *J Energy Chem.* 2020;43:182-187.
44. Huang Y, Li Z, Jin S, et al. Carbon nanohorns/nanotubes: an effective binary conductive additive in the cathode of high energy-density zinc-ion rechargeable batteries. *Carbon.* 2020;167:431-438.
45. Huang J, Wang Z, Hou M, et al. Polyaniline-intercalated manganese dioxide nanolayers as a high-performance cathode material for an aqueous zinc-ion battery. *Nat Commun.* 2018;9(1):1-8.
46. Zeng Y, Zhang X, Meng Y, et al. Achieving ultrahigh energy density and long durability in a flexible rechargeable quasi-solid-state Zn-MnO<sub>2</sub> battery. *Adv Mater.* 2017;29(26):1700274.
47. Liu Y, Chi X, Han Q, et al.  $\alpha$ -MnO<sub>2</sub> nanofibers/carbon nanotubes hierarchically assembled microspheres: approaching practical applications of high-performance aqueous Zn-ion batteries. *J Power Sources.* 2019;443:227244.
48. Xu J-W, Gao Q-L, Xia Y-M, et al. High-performance reversible aqueous zinc-ion battery based on iron-doped alpha-manganese dioxide coated by polypyrrole. *J Colloid Interface Sci.* 2021;598:419-429.
49. Wang L, Zhang Y, Hu H, et al. A Zn(ClO<sub>4</sub>)<sub>2</sub> electrolyte enabling long-life zinc metal electrodes for rechargeable aqueous zinc batteries. *ACS Appl Mater Interfaces.* 2019;11(45):42000-42005.
50. Li Z, Huang Y, Zhang J, et al. One-step synthesis of MnO<sub>x</sub>/PPy nanocomposite as a high-performance cathode for a rechargeable zinc-ion battery and insight into its energy storage mechanism. *Nanoscale.* 2020;12(6):4150-4158.
51. Huang Y, Mou J, Liu W, et al. Novel insights into energy storage mechanism of aqueous rechargeable Zn/MnO<sub>2</sub> batteries with participation of Mn<sup>2+</sup>. *Nano-Micro Lett.* 2019;11(1):1-13.
52. Wang J, Shen Z, Yi M. Liquid-exfoliated graphene as highly efficient conductive additives for cathodes in lithium ion batteries. *Carbon.* 2019;153:156-163.
53. Mo F, Liang G, Meng Q, et al. A flexible rechargeable aqueous zinc manganese-dioxide battery working at -20°C. *Energy Environ Sci.* 2019;12(2):706-715.
54. Chen S, Zhang Y, Geng H, et al. Zinc ions pillared vanadate cathodes by chemical pre-intercalation towards long cycling life and low-temperature zinc ion batteries. *J Power Sources.* 2019;441:227192.
55. Li X, Ma L, Zhao Y, et al. Hydrated hybrid vanadium oxide nanowires as the superior cathode for aqueous Zn battery. *Mater Today Energy.* 2019;14:100361.
56. Quan Y, Chen M, Zhou W, et al. High-performance anti-freezing flexible Zn-MnO<sub>2</sub> battery based on polyacrylamide/graphene oxide/ethylene glycol gel electrolyte. *Front Chem.* 2020;8:1-9.
57. Zhang J, Wang M, Zeng M, et al. Sulfite modified and ammonium ion intercalated vanadium hydrate with enhanced redox kinetics for aqueous zinc ion batteries. *J Power Sources.* 2021;496:229832.
58. Mo F, Liang G, Wang D, et al. Biomimetic organohydrogel electrolytes for high-environmental adaptive energy storage devices. *EcoMat.* 2019;1(1):e12008.

## SUPPORTING INFORMATION

Additional supporting information may be found in the online version of the article at the publisher's website.

**How to cite this article:** Yang G, Huang J, Wan X, et al. An aqueous zinc-ion battery working at -50°C enabled by low-concentration perchlorate-based chaotropic salt electrolyte. *EcoMat.* 2022;e12165. doi:10.1002/eom2.12165